

Title: Mixed IgG Fc immune complexes exhibit blended binding profiles and refine FcR affinity estimates

Authors: Zhixin Cyrillus Tan¹, Anja Lux², Markus Biburger², Prabha Varghese², Stephen Lees³, Falk Nimmerjahn², Aaron S. Meyer^{1,3,4,5,*}

5 Affiliations:

¹ Bioinformatics Interdepartmental Program, University of California, Los Angeles (UCLA)

² Department of Genetics, Friedrich-Alexander-University of Erlangen-Nürnberg

³ Department of Bioengineering, UCLA

⁴ Jonsson Comprehensive Cancer Center, UCLA

10 ⁵ Eli and Edythe Broad Center of Regenerative Medicine and Stem Cell Research, UCLA

*Corresponding author. Email: ameyer@asmlab.org

Abstract: Immunoglobulin (Ig)G antibodies coordinate immune effector responses by selectively binding to target antigens and then interacting with various effector cells via the Fcγ receptors. The Fc domain of IgG can promote or inhibit distinct effector responses across several different immune cell types through variation based on subclass and Fc domain glycosylation. Extensive characterization of these interactions has revealed how the inclusion of certain Fc subclasses or glycans results in distinct immune responses. During an immune response, however, IgG is produced with mixtures of Fc domain properties, so antigen-IgG immune complexes are likely to almost always be comprised of a combination of Fc forms. Whether and how this mixed composition influences immune effector responses has not been examined. Here, we measured Fcγ receptor binding to immune complexes of mixed Fc domain composition. We found that the binding properties of the mixed-composition immune complexes fell along a continuum between those of the corresponding pure cases. Binding quantitatively matched a mechanistic binding model, except for several low-affinity interactions mostly involving IgG2. We found that the affinities of these interactions are different than previously reported, and that the binding model could be used to provide refined estimates of these affinities. Finally, we demonstrated that the binding model can predict effector-cell elicited platelet depletion in humanized mice, with the model inferring the relevant effector cell populations. Contrary to the previous view in which IgG2 poorly engages with effector populations, we observe appreciable binding through avidity, but insufficient amounts to observe immune effector responses. Overall, this work demonstrates a quantitative framework for reasoning about effector response regulation arising from IgG of mixed Fc composition.

Summary points

- 35 • The binding behavior of mixed Fc immune complexes is a blend of the binding properties for each constituent IgG species.
- An equilibrium, multivalent binding model can be generalized to incorporate immune complexes of mixed Fc composition.
- Particularly for low-affinity IgG-Fcγ receptor interactions, immune complexes provide better estimates of affinities.
- 40 • The FcγR binding model predicts effector-elicited cell clearance in humanized mice.

Introduction

Antibodies are both a core component of adaptive immunity and a versatile platform for developing therapies. An antibody's role in promoting immunity is defined by its selectivity
45 toward a target antigen, as determined by its variable region, and its ability to elicit effector cell responses, defined by the composition of its constant, fragment crystallizable (Fc) region. Antibodies of the IgG type direct effector response by binding to the Fc γ receptor (Fc γ R) family via their Fc-portion. Fc γ R activation is initiated through IgG-mediated clustering, which in turn is caused by the engagement of several antibodies on an antigen
50 target forming an immune complex (IC). Depending upon the receptors included, this interaction may promote or prevent an effector response. This clustering mechanism ensures that more than one IgG is present whenever effector responses occur.

The immune response triggered by an IgG IC consisting of a specific Fc form, including subclass or glycosylation, is defined by its binding to specific Fc γ receptors, each of which
55 differs in signaling effect and expression patterns¹. Consequently, accurate estimates of IgG Fc-Fc γ R affinities are essential to understanding their effect. Most existing Fc γ R affinity measurements have been performed by surface plasmon resonance (SPR) using monovalent IgG^{2,3}. SPR accurately assesses protein-protein binding kinetics, but many antibody-Fc receptor interactions are weak enough to fall outside the assay's quantitative
60 range when assessed in monovalent form. Clustering leads to avidity effects, wherein even weak interactions can cooperatively lead to strong binding⁴. Indeed, avidity is widely employed in natural and engineered systems to promote binding through low-affinity interactions⁵. Therefore, direct measurement of IC binding might more accurately quantify IgG Fc properties, particularly for low-affinity interactions. Measuring Fc binding as
65 multivalent ICs additionally resembles the relevant *in vivo* context of effector responses⁶.

Physiological antibody responses universally involve Fc mixtures. For instance, during the course of infection, the composition of IgG subclasses shifts dynamically to different subclasses due to class switching⁷. Even when recombinantly manufacturing monoclonal therapeutic antibody preparations, heterogeneity exists in the glycosylation forms derived,
70 and this glycan heterogeneity likely exists during endogenous antibody production as well^{8,9}. With a mixture of antibodies of different Fc compositions but identical antigen

binding, there might be an additive combination of effect, or a minor species (e.g., glycosylation variant) might present an outsized effect promoting or preventing effector responses. Therefore, knowledge of how these different forms influence the behavior of one another would allow one to modulate immune responses by adjusting the combination of different subclasses. With respect to therapeutic monoclonal antibody preparations, this would help guide the evaluation of biosimilars by determining whether glycosylation forms present at small fractions might influence overall therapeutic efficacy¹⁰.

After binding to Fc receptors, effector cell-elicited responses to IgG include several different functionally distinct mechanisms, including antibody-dependent cell cytotoxicity (ADCC) and phagocytosis (ADCP). Effector responses are coordinately regulated by the cell types present within a tissue^{11,12}, the FcγRs expressed on those effector cells¹³, the Fc properties present within an immune complex¹, and properties of antigen engagement^{14,15}. Regulation at the Fc receptor and cell population level is a challenge to engineering antibodies with desirable cell-killing functions, as well as understanding both productive and pathogenic immune responses. Furthermore, it has become clear that in addition to NK cells, tissue-resident macrophages and bone marrow-derived monocytes participate in cytotoxic antibody-dependent target cell clearance. In contrast to NK cells (expressing only one activating FcγR, FcγRIIIA), these myeloid cell subsets express a broader set of activating FcγRs and the inhibitory FcγRIIB¹³. Thus, mixed IC may trigger all or specific subsets of activating/inhibitory FcγRs, resulting in further complexity. Despite the presence of and capacity to bind to multiple activating FcγRs on myeloid effector cells, our previous studies have demonstrated that individual IgG subclasses, such as mIgG2a/c for example, may mediate their activity through select activating FcγRs, indicating that there may be specialization in FcγR signaling⁶.

Our team recently demonstrated that a model of IC-FcγR binding accurately captured and could predict *in vitro* binding across various IgG isotypes¹⁶. Further, it could accurately predict antibody-elicited tumor cell killing in mice across antibodies of varied isotype, glycosylation status, and FcγR knockouts¹⁶. Directly quantifying and predicting cell clearance makes it possible to accurately anticipate and optimize for antibody-mediated therapeutic effects. However, it is still unclear whether such a modeling strategy can accurately predict the response of human immune cells, particularly given the divergent

properties between the murine and human receptors^{17–19}, and whether this modeling strategy can extend to ICs of mixed composition.

105 Here, we examined the binding properties of ICs with mixed IgG Fc composition. We quantified the binding of these ICs to each individual FcγR and observed that mixed-composition ICs resulted in a continuum of binding responses. A multivalent binding model extended to hetero-valent immune complex mixtures captured binding overall. However, surprisingly, it did not match certain low-affinity interactions²⁰. Investigating the source of
110 this discrepancy allowed us to improve the estimates of these interactions' affinities. We additionally demonstrate that the binding model can be used to both predict *in vivo* effector responses in humanized mice and infer the cell types responsible for these responses. Thus, while antibody effector responses operate through a complex milieu of antibody species, Fc receptors, and cell types, IC profiling paired with modeling provides a
115 framework to reason about the role of each molecular and cellular element.

Results

Profiling the binding effects of mixed-composition immune complexes

To determine the effect of having multiple Fc forms present within an immune complex (IC), we developed a controlled and simplified *in vitro* system. Like in previous work, we
120 employed a panel of CHO cell lines expressing one of six individual human FcγRs¹⁶ (Fig. 1a). ICs were formed by immobilizing anti-2,4,6-trinitrophenol (TNP) human IgG on conjugates of TNP and bovine serum albumin (TNP-BSA) with an average valency of 4 or 33. IgG binding was then quantified after incubation with the cells, using a constant IC concentration of 1 nM (Fig. S1). In contrast to our previous work using a single IgG
125 isotype, we assembled ICs from mixtures of each IgG isotype pair¹⁶. For each pair of IgGs, ICs were formed with a spectrum of six compositions of the IgG pair, including 100%/0%, 90%/10%, and 67%/33% mixtures. Combinations of 6 FcγRs, 2 valencies, 6 IgG pairs, and 6 IgG compositions resulted in 432 distinct experimental conditions. One-way ANOVA showed that more than 70% variance in the data are between experimental conditions
130 rather than within them, indicating that more than 70% of the variance could be explained by biological differences. This suggests that, within each condition, measurements were consistent (Tbl. S1).

Inspection of the resulting binding data revealed several expected patterns. Among the conditions with only one IgG present, the measured binding showed a strong, positive correlation with the documented IgG-FcγR interaction affinities (Fig. 1b). The higher valency ICs universally showed greater binding signal compared to their matching lower-valency counterparts, and there is an obvious negative trend between documented affinities and the ratio between the 33-valent and 4-valent complex binding (Fig. 1c). This trend is expected since, although complexes of both valencies can bind densely with high-affinity units, only high-valent complexes compensate for low affinity through avidity⁴. Therefore, while high-affinity complexes result in greater binding, low-affinity complexes have greater intervalency binding ratios. Finally, mixtures spanning 100% of one IgG isotype to another generally showed a monotonic shift with composition (Fig. S1). These patterns, along with their reproducibility (Tbl. S1), gave us confidence in the quality of the binding measurements.

We also observed several unexpected trends among the binding measurements. There was appreciable binding from IgG2-FcγRI interactions, despite this combination being reported as non-binding³ (Fig. 1d). We also saw an increase in binding along the shift from IgG4 to IgG1 with FcγRIIIA-158F, even though these two isotypes are documented to have identical affinity³ (Fig. 1e). These two observations are consistent with previous binding measurements using the same TNP-based IC system¹⁶.

To better visualize the binding measurements, we performed principal component analysis (PCA) on the median measurement of each condition, with each isotype mixture and valency as a sample and each receptor as a feature. The first principal component (PC1) explains more than 86% of the variance, and the first two components (PC1 and PC2) explain 93% (Fig. 2a). Inspecting the scores, we found that the 33-valent measurements are more broadly distributed, consistent with their greater expected binding (Fig. 2b/c). PC1 mostly separates IgG3 binding from other isotypes, reflecting that IgG3 has the greatest binding among IgG subclasses (Fig. S1). PC2 separated the genotype variants of FcγRIIA and FcγRIIIA and associated most strongly with IgG3 and IgG4 (Fig. 2d), reflecting that these two subclasses showed larger differences in binding with genotype (Fig. S1).

In all, these data support that TNP-assembled ICs provide a controlled *in vitro* system in which we can profile the effects of mixed IC composition on binding to effector cell populations. Quantifying binding using ICs may, in fact, provide more precise quantification of IgG-Fc γ R interaction affinities, particularly for lower affinity pairs, and mixed Fc composition ICs showed binding between that of the corresponding single Fc cases.

A multivalent binding model accurately predicts *in vitro* IgG mixtures binding and updates Fc-Fc γ R affinities

To model the effects of polyclonal antibody responses, we extended a simple, equilibrium binding model that we have previously used to model antibody effector response^{16,20}. Briefly, immune complexes are assumed to bind to Fc γ Rs on the cell surface with monovalent binding kinetics, and then can engage additional receptors with a propensity proportional to their affinity (Fig. 3a). Though additional assumptions are not required for modeling ICs of mixed isotype composition, this extension leads to a large combinatorial expansion in the number of binding configurations. Through some properties of combinatorics, we derived simplified expressions for many macroscopic quantities to allow this model to scale to multi-ligand, multi-receptor, and multivalent situations²⁰.

We first used the measured receptor expression (Tbl. S2) and documented affinities³ with the model and obtained reasonable agreement overall (Fig. 3c). While the predicted values mostly agreed with the measurements, there were several notable outliers, most prominently an underestimate of IgG2-Fc γ RI binding (Fig. 3c, red circle). To improve the measurement fit, we reversed the estimation process and used the measured binding to infer the interaction affinities via Markov chain Monte Carlo (MCMC) (Fig. 3b). We first created a baseline fit quality by fitting all but the affinities (e.g., receptor abundance and the crosslinking parameter K_x^* , Fig. 3d). Although the fit improved, outliers persisted (circled in red in Fig. 3d). Therefore, we next performed the fitting while allowing the Fc-Fc γ R affinities to vary. Although we only used the single-IgG measurements to infer the Fc affinities (Fig. 3e), we obtained much more accurate predictions for all measurements of both single and mixed IgG compositions (Fig. 3f).

To further confirm the generality of these updated affinities, we validated these new affinity estimates with an independent dataset collected in a previous study¹⁶. This previous study independently measured the binding of BSA-TNP complexes *in vitro* with two distinct

195 average valencies (4 and 26), but only the binding of single IgG isotypes. We set the Fc affinities to either documented or updated values and let MCMC fit the other parameters. The new affinities resulted in a vastly improved agreement with the data (Fig. 3g/h).

To illustrate the impact of the affinity changes, we compared the binding predictions with two sets of affinities (Fig. S2/S3) to their corresponding measurements (Fig. S1). For FcγRI binding to IgG2-IgG4 mixtures, the experiment indicated that there is still notable
200 binding with mostly or 100% IgG2, while IgG2-FcγRI was documented as non-binding³. The updated values amended the prediction and reflected this interaction, especially for the 33-valent complex (Fig. 3i/j, green circle). For FcγRIIB-232I binding to IgG3-IgG4, the documented affinities indicated there should be more binding to IgG4 compared to IgG3, contrary to our observation (Fig. 3k). The updated affinities instead accurately predicted
205 the binding of all mixtures at both valencies (Fig. 3l). These examples demonstrate that the affinity adjustments greatly improved agreement with the binding measurements.

As our Fc affinity inference was constructed in a Bayesian fashion, both the prior (documented) and the posterior (updated) affinity values are represented as distributions accounting for uncertainty. Inspecting these updated distributions (Fig. 4a–d; Tbl. S3), we
210 noted several trends. The model made the largest adjustments to the Fc affinities of IgG2 (Fig. 4b), followed by IgG4 (Fig. 4d). Most IgG1 (Fig. 4a) and IgG3 (Fig. 4c) affinities remained unmodified, except for a slight increase in their FcγRIIB-232I affinities. The most notable update occurred to IgG2-FcγRI. Previously reported as nonbinding, FcγRI was revised to be the highest affinity receptor for IgG2, consistent with the receptor's high
215 affinity to other human IgG subclasses. This discrepancy was reflected in the model prediction before affinity fitting, where the IgG2-FcγRI binding was the striking outlier (Fig. 3d/g). Another significant adjustment occurred with IgG3-FcγRIIB-232I. Although FcγRIIB-232I has a low affinity for all IgG subclasses, our update led to IgG3 being the strongest-binding subclass (Fig. 4c, S2 & S3). More subtle differences can be observed from specific
220 model predictions (Fig. S2 & S3). The revised affinities showed a similar overall correlation with binding overall (Fig. 4e). The inter-valency binding ratios show a more prominent negative correlation, however, due to the movement of the IgG2-FcγRI outlier (Fig. 4f).

Multivalent binding predicts antibody-elicited effector responses in humanized mice

We next sought to link the binding of ICs to their effects on the clearance of antigen targets
225 *in vivo*. To quantify the antibody-driven activity of each effector cell, we first measured the
binding of each human IgG subclass to immune effector cells *in vitro* in IC of two
valencies, 4 and 33 (Fig. 5a–d). The measurements show that the binding amounts of
IgG1 and IgG3 were generally about 10-fold higher in magnitude than those of IgG2 and
IgG4. For the latter two subclasses, their 4-valent complex binding was almost negligible.
230 In all cases except IgG2, neutrophils had more binding than classical and nonclassical
monocytes.

We predicted the same quantities of IC binding by the multivalent binding model with either
the previously documented³ or updated affinities (Tbl. S4), and the quantification of FcγR
abundance¹³ (Tbl. S6, Fig. 5e–h). These estimated binding amounts broadly aligned with
235 the measurements. Between the two sets of affinities, the predictions for IgG1 and IgG3
remained almost identical (Fig. 5e/g), while some differences were reflected in IgG2 and
IgG4 (Fig. 5f/h), consistent with the affinities changing more for IgG2 and IgG4 (Fig. 4a–d).
Most prominently, the predicted binding to nonclassical and classical monocytes was
adjusted to be much higher for 33-valent IgG2 (Fig. 5f), better matching the measured
240 values (Fig. 5b). These changes indicate that the updated affinities better predict IgG IC
binding to effector cells, suggesting that they may also help improve the estimation of *in
vivo* cell response.

Next, we used the multivalent binding model with regression to predict *in vivo* antibody
effector cell-driven platelet depletion in humanized mice. In the process of extending our
245 previous model, we elected to use the cumulative density function of the exponential
distribution as the link function in our generalized linear regression model to link the overall
cell activity to the amount of target (e.g., platelet) depletion (Fig. 6a). Since the cell
depletion effects have a limited range—one cannot deplete an antibody target of more
than 100% or less than 0%—we must use a non-linear link function to transform the linear
250 combination. While many functions provide this general relationship (such as the
hyperbolic tangent function used before¹⁶), we realized that the extent of target cell
depletion can be thought of as a form of survival analysis. In other words, given a certain
antibody activity, a target cell has a certain probability of being cleared within the given

timescale of the experiment. Assuming all target cells have an equal propensity of being
255 cleared dictates an exponential relationship for the link function²¹.

Having refined the cell clearance model, we applied it to a previously-collected dataset
examining platelet depletion in humanized mice²². After fitting the cell type weighting, we
found the model fit the experiments well, especially considering the experiment-to-
experiment variability due to donor graft variation and other sources of experimental
260 uncertainty (Fig. 6b/c). The fitting was almost identical when using documented (Fig. 6b) or
updated (Fig. 6c) FcγR affinities.

A benefit of the generalized linear regression model is that it provides an easy
interpretation of each component. Inspecting the cell type weights, we found that classical
monocytes were inferred to be the predominant effector cell type (Fig. 6d/e). IgG2 had
265 some binding to each effector cell type, but no activity was inferred whatsoever (Fig. 5f,
6d/e). As the affinity updates are most relevant to IgG2, and this isotype had no *in vivo*
effect, it is reasonable that these changes had little effect on agreement with the data (Fig.
5f, 6e). While classical monocytes were inferred to exert the greatest impact on platelet
depletion across isotypes, neutrophils, not classical monocytes, had the greatest binding
270 (Fig. 5a–d). This demonstrates that the most bound cell type does not equate to the most
potent effector. The regression model can incorporate the molecular level binding
estimation and the depletion outcome to provide insights into the overall potency of each
cell type. Overall, we found that the binding model could predict antibody-elicited effector
responses *in vivo* in humanized mice.

275 Discussion

In this work, we explored the binding properties of ICs with mixed IgG Fc composition and
linked their *in vitro* effects to *in vivo* effector cell-elicited platelet depletion. To quantify the
binding of mixed IgG ICs *in vitro*, we measured every human IgG subclass pair across a
range of compositions multimerized at two different valencies (Fig. 1). Fitting these
280 measurements to a model of multivalent interactions using documented affinities for each
interaction, our model captured overall binding trends, with some outliers (Fig. 3). We
uncovered that the model discrepancies could be explained by inaccurate estimates of
especially low-affinity Fc receptor interactions, most prominently involving IgG2. We

validated revised affinities within an independent dataset and found it greatly improved
285 concordance with the data there as well. Finally, we used measurements of binding to
effector cell populations to predict *in vivo* antibody-driven depletion of platelets in
humanized mice (Fig. 5 & 6). While the updated affinities did not change the agreement of
the model with the data, it did change the interpretation of IgG2's small effect on
290 depletion—rather than not binding to classical monocytes, IgG2 binds strongly when in a
larger IC, but platelets might provide insufficient avidity to observe sufficient engagement
(Fig. 6).

Considering that polysaccharide antigens present during bacterial infections or upon
vaccination efficiently trigger IgG2 responses²³, our data would support the notion that
FcyR-dependent effector functions such as phagocytosis of opsonized bacteria may
295 contribute to protective IgG responses in humans more than expected. Reversely,
autoreactive IgG2 responses observed during many autoimmune diseases may contribute
to autoimmune pathology via FcyRs, which may warrant to develop therapeutic
interventions blocking this pathway also in IgG2-dominated autoimmune diseases²⁴.
Finally, with respect to the use of human IgG2 antibody formats as immunomodulatory
300 antibodies for the therapy of cancer, our results would support strategies to engineer IgG2
variants with reduced binding to activating FcyRs and optimized binding for the inhibitory
FcyRIIb, which has been shown to be critical for immunomodulatory IgG activity to further
improve their therapeutic activity and reduce unwanted side-effects²⁵.

IgG subclasses and glycan variants are defined by their differing affinity toward each Fc
305 receptor^{3,19,26}. Therefore, accurate measurements of each Fc receptor affinity are critical to
understanding the differences in immune responses to each IgG. Using a mechanistic
multivalent binding model alongside *in vitro* binding fluorescence measurements, we were
able to derive a new set of Fc affinities distinct from those measured by surface plasmon
resonance (SPR). Due to the heightened avidity, we found that multivalent ICs are better
310 at detecting low-affinity IgG-Fc receptor interactions (Fig. 4b). Examining binding through
ICs also better simulates the relevant structure of Fc-FcR interactions *in vivo*. Harnessing
avidity to overcome the low affinity of interactions is a common theme in immunology and
its experimental characterization. For instance, tetramers are routinely used for isolating

antigen-selective T cells²⁷. Here, we additionally show that these complexes can be used
315 alongside quantitative models to infer properties of these systems.

Our results suggest that, within ICs comprised of several distinct subclasses or
glycosylation variants, the Fc interaction effects are a blend of the constituent species'
properties. This means that ICs' most extreme binding and effector responses should
predominantly arise from whichever species is most potent in soliciting binding or a
320 response. It also should provide some encouragement that the effector responses elicited
from therapeutic antibodies should vary roughly in proportion to their relative composition,
and small contaminants of alternative Fc subclasses or glycosylation can only have a
substantial effect if those species differ extremely in their responses alone. One caveat of
this observation is that we only examined mixtures of antibodies with differing Fcs but
325 identical antigen binding—polyclonal mixtures of antibodies will have still other interaction
effects, in part because antigens can form a higher valency complex when they are
present in combination²⁸. While in this work we only demonstrated Fc subclasses mixtures,
the same lessons likely apply to glycosylation mixtures, both *in vitro* and *in vivo*, since
different subclasses and glycosylation variants exert their effect through divergent affinities
330 toward Fc receptors.

Fc receptor-mediated effects are central to protection from both endogenously produced
and therapeutic antibodies. Our work demonstrates that computational methods greatly
facilitate reasoning about the complex signaling of the Fcγ receptor pathway quantitatively
and at both cellular and organismal levels. This work extends our previous modeling to the
335 depletion of platelets as a target and humanized mice¹⁶. Humanized mice serve as an
ideal surrogate for understanding human immunity²⁹. However, this model system is
complicated by graft-to-graft differences, including the level of humanization and genetic
heterogeneity of human stem cell donors²⁹. The depletion data reflected these
complications, with high donor-to-donor and mouse-to-mouse variation²² (Fig. 6b/c). We
340 anticipate that mechanistic models of antibody-mediated protection, such as the one here,
will continue to grow in their utility for studying model systems such as humanized mice. In
fact, as other features of antibodies are incorporated, such as variation in antigen
specificity, it may become possible to connect behavior *in vitro* all the way to protection in
human subjects^{30,31}.

345 **Methods**

Data and Software Availability

All analysis was implemented in Julia and can be found at <https://github.com/meyer-lab/FcRegression.jl>.

Chinese hamster ovary (CHO) cell FcγR Expression Quantitation

350 Human FcγR expression on stably transfected CHO cells was quantified by determining the antibody binding capacity (ABC) for antibodies specific for the respective Fcγ receptor (Tbl. S2)¹³. Quantum Simply Cellular (QSC) anti-mouse beads (Bangs Laboratories Ltd.) with known binding capacities for mouse IgG were used according to manufacturer's instructions. Subsequently, a reference curve was generated by correlating the
355 fluorescence intensity (caused by the respective anti-FcγR antibody) and the number of antibody binding sites of the different QSC beads. This reference curve was established in each experiment for all FcγR-specific antibodies of interest (PE-conjugated clone 10.1 to detect FcγRI, clone AT10 to detect FcγRIIa/b and clone 3G8 to detect FcγRIIIa, all from Biolegend) and used to calculate receptor numbers based on fluorescence intensity of
360 FcγR staining on CHO cells. Samples were measured on a FACSCantoll flow cytometer and analyzed with FACSDiva software.

Generalized multi-ligand, multi-receptor multivalent binding model

To model polyclonal antibody-antigen immune complexes (ICs), we employed a multivalent binding model to account for ICs of mixed IgG composition previously
365 developed and detailed in Tan and Meyer²⁰.

In this model, we define N_L as the number of distinct monomer Fc's and N_R as the number of FcRs, and the association constant of monovalent Fc-FcR binding between Fc i and FcR j as $K_{a,ij}$. Multivalent binding interactions after the initial interaction are assumed to have an association constant of $K_x^* K_{a,ij}$, proportional to their corresponding monovalent
370 affinity. The concentration of complexes is L_0 , and the complexes consist of random ligand monomer assortments according to their relative proportion. The proportion of ligand i among all monomers is C_i . By this setup, we know $\sum_{i=1}^{N_L} C_i = 1$. $R_{\text{tot},i}$ is the total number of

receptors i expressed on the cell surface (where this term is used synonymously for the actual determined number of binding sites for the respective anti-FcR antibodies), and $R_{\text{eq},i}$ the number of unbound receptors i on a cell at the equilibrium state during the ligand complex-receptor interaction.

The binding configuration at the equilibrium state between an individual complex and a cell expressing various receptors can be described as a vector $\mathbf{q} = (q_{10}, q_{11}, \dots, q_{1N_R}, q_{20}, \dots, q_{2N_R}, q_{30}, \dots, q_{N_L N_R})$ of length $N_L(N_R + 1)$, where q_{ij} is the number of ligand i bound to receptor j , and q_{i0} is the number of unbound ligand i on that complex in this configuration. The sum of elements in \mathbf{q} is equal to f , the effective avidity. For all i in $\{1, 2, \dots, N_L\}$, let $\varphi_{ij} = R_{\text{eq},j} K_{a,ij} K_x^* C_i$ when j is in $\{1, 2, \dots, N_R\}$, and $\varphi_{i0} = C_i$. Then, the relative number of complexes in the configuration described by \mathbf{q} at equilibrium is

$$v_{\mathbf{q},\text{eq}} = \binom{f}{\mathbf{q}} \frac{L_0}{K_x^*} \prod_{i=1, j=0}^{i=N_L, j=N_R} \varphi_{ij}^{q_{ij}},$$

with $\binom{f}{\mathbf{q}}$ being the multinomial coefficient. Then the total relative amount of bound receptor type n at equilibrium is

$$R_{\text{bound},n} = \frac{L_0 f}{K_x^*} \sum_{m=0}^{N_L} \varphi_{mn} \left(\sum_{i=1, j=0}^{i=N_L, j=N_R} \varphi_{ij} \right)^{f-1}.$$

By conservation of mass, we know that $R_{\text{tot},n} = R_{\text{eq},n} + R_{\text{bound},n}$ for each receptor type n , while $R_{\text{bound},n}$ is a function of $R_{\text{eq},n}$. Therefore, each $R_{\text{eq},n}$ can be solved numerically from its $R_{\text{tot},n}$ measured experimentally. Similarly, the total relative number of complexes bind to at least one receptor on the cell is

$$L_{\text{bound}} = \frac{L_0}{K_x^*} \left[\left(\sum_{i=1, j=0}^{i=N_L, j=N_R} \varphi_{ij} \right)^f - 1 \right].$$

FcRs are activated through crosslinking. The amount of each kind of receptor in a multimerized complex can be calculated as

$$R_{\text{multi},n} = \frac{L_0 f}{K_x^*} \sum_{m=1}^{N_L} \varphi_{mn} \left[\left(\sum_{i=1, j=0}^{i=N_L, j=N_R} \varphi_{ij} \right)^{f-1} - 1 \right].$$

Immune Complex Binding Measurement

Chinese hamster ovary (CHO) cells stably expressing human FcγRs were used to assess IgG-IC binding to hFcγRs as previously described⁶. Briefly, ICs were generated by coincubation of 10 μg/ml anti-TNP human IgG subclasses (clone 7B4) and 5 μg/ml BSA
400 coupled with either an average of 4 or 33 TNP molecules (Biosearch Technologies) to mimic low or high valency ICs, respectively, for 3 h with gentle shaking at room temperature. To address the impact of distinct subclass combinations on hFcγR binding, human IgG1 through IgG4 subclasses were mixed at specific conditions (100%, 90%, 66%, 33%, 10% of one subclass filled up to 10μg/ml with the respective second subclass)
405 before the addition of TNP-BSA. ICs were subsequently incubated with 100,000 FcγR expressing or untransfected control CHO cells for 1 h under gentle shaking at 4°C. Bound ICs were detected using a PE-conjugated goat anti-human IgG F(ab')₂ fragment at 0.5 μg/ml (Jackson ImmunoResearch Laboratories) on a BD FACSCanto II flow cytometer. Each IC binding measurement was normalized to the average of all the points within that
410 replicate.

Alternatively, binding to human primary peripheral blood leukocytes co-expressing specific FcγRs was studied. Blood was drawn from healthy volunteers with informed consent of the donor and the local ethical committee. Erythrocytes were lysed by the addition of ddH₂O for 30 sec at room temperature to obtain total leukocytes. Immune complexes were
415 generated as described above and incubated with 200,000 leukocytes. Leukocyte subpopulations were identified by staining of cell-type-specific surface markers. Fluorescently labeled antibodies PE/Cy7-conjugated anti-CD19, PerCP-conjugated anti-CD3, APC-conjugated anti-CD33, Brilliant Violet 510 conjugated anti-CD14, FITC-conjugated anti-CD56 and APC-Fire 750 conjugated anti-CD45 were obtained from
420 Biologend.

The cell identification strategy was as follows: aggregates of cells were excluded by their forward light scatter (FSC) characteristics (area vs. height) and dead cells based on staining with DAPI. Leukocytes were identified by expression of common leukocyte marker CD45. Among those, neutrophils were gated based on high side light scatter (SSC)
425 characteristics and lack of surface CD14 and classical monocytes based on intermediate SSC and expression of CD14. Within the CD14⁻SSC^{low} cells, B and T cells were gated by

expression of CD19 or CD3, respectively. Staining of CD56 was used to distinguish NK cells. The remaining CD33 expressing cells are gated as non-classical monocytes.

430 Data were analyzed with FlowJo or FACSDiva Flow Cytometry Analysis Software. The relative fluorescence units were normalized so that measurements of each day have geometric means of 1.0. The variance explained calculated for principal component analysis was defined as $1 - \frac{\|X - \hat{X}\|_F^2}{\|X\|_F^2}$, where $\|\cdot\|_F^2$ indicates the Frobenius norm.

Immune Complex Binding Analysis

435 Fitting the parameters in the binding quantification was performed by Monte Carlo Markov Chain (MCMC) implemented by Turing.jl³².

At first, we plugged in the documented values into the binding model for all parameters without fitting, thus the geometric means of CHO cell receptor expression (Tbl. S2), documented affinities³, nominal valencies (4 and 33), and K_x^* as $6.31 \times 10^{-13} \text{ cell} \cdot \text{M}^{16}$, as estimated in previous work (Fig. 3c)³³. To examine the role of affinity fitting, we used 440 MCMC to fit all parameters except (Fig. 3d) and including (Fig. 3e) affinities. CHO receptor prior distributions were inferred from their measured values through maximal likelihood estimation (MLE) in Distributions.jl³⁴ for both IgG mixture dataset (Tbl. S2) and validation Robinett et al.³³ dataset (Tbl. S5). The affinity priors were inferred from documented Fc affinities and standard errors with these rules: (1) each prior follows a lognormal 445 distribution; (2) the mode of the distribution is the documented value, and the interquartile range of the distribution is the standard error; (3) if the values of mode or standard errors are too small, the mode was clipped to $1 \times 10^4 \text{ M}^{-1}$, and the interquartile range was clipped to $1 \times 10^5 \text{ M}^{-1}$ to deal with recorded nonbinding cases^{3,35}. The priors of valencies and crosslinking constant were as follows

450
$$f_4 \sim \text{logN}(\mu = \log(4), \sigma = 0.2),$$

$$f_{33} \sim \text{logN}(\mu = \log(33), \sigma = 0.2),$$

$$K_x^* \sim \text{logN}(\mu = \log(6.31 \times 10^{-13}), \sigma = 2.0).$$

MCMC was initialized with the maximum a posteriori estimation (MAP) optimized by a limited-memory BFGS algorithm implemented by Optim.jl³⁶, then sampled through a No U-Turn Sampler (NUTS) implemented by Turing.jl³².
455

***In vivo* Regression Model**

We extended the *in vivo* antibody-elicited target cell depletion regression model with both cell type weights and FcγR weights (Fig. 6a). Depletion, y , was represented as the percent reduction in the number of target cells.

460 To quantify the activity of each effector cell, we first used the multivalent binding model to predict the amount of multimerized FcγR of each kind, $R_{\text{multi},i}$, assuming each IC is 4-valent. Then the activity of this cell type is assumed to be a linear combination of these predictions and a set of cell type weights, p_i , that are set to either +1 or -1 for activating or inhibitory receptors, respectively, clipped to 0 if it is negative:

$$465 \quad x_n = \max(p_1 R_{\text{multi},1} + p_2 R_{\text{multi},2} + \dots, 0).$$

To determine how these cell types bring the depletion effect at the organism level, we combine their estimated effects, x_n , with a weighted sum, where we introduce another set of weights, w_n , that are specific to each cell type. To convert the activities to a limited range of depletion, (i.e., one cannot have a reduction over 100%), the regression was
470 transformed by an exponential linker function (the cumulative density function of exponential distribution) such that the predicted effectiveness: $\hat{y} = F_{\text{exp}}(wx) = 1 - \exp(-wx)$ so that $\lim_{x \rightarrow \infty} F_{\text{exp}}(X) = 1$. Together, we have the estimated depletion as

$$\hat{y} = F_{\text{exp}}(w_1 x_1 + w_2 x_2 + \dots).$$

We did not estimate the amount of each cell type in an individual, nor did we include them
475 in the model, because the weights, w_n , were supposed to absorb these quantities, while requiring effector cell abundance can limit the application of this model to specific organs where the tissue resident cell abundance cannot be accurately quantified.

The regression against *in vivo* effectiveness of IgG treatments was performed via Monte Carlo Markov Chain (MCMC) implemented by Turing.jl³². For the multivalent binding
480 model, the ligand concentration was assumed to be 1 nM and valency to be 4. The

receptor expression level was set to the geometric means of the values measured in previous work (Tbl. S6)¹³. For the receptor weights, p_i , we set the weight of the only inhibitory receptor, FcγRIIB, as -1.0 , while every activating receptor to be $+1.0$.

485 MCMC was initialized with the maximum a posteriori estimation (MAP) optimized by a limited-memory BFGS algorithm implemented by Optim.jl³⁶, then sampled through a No U-Turn Sampler (NUTS) implemented by Turing.jl³².

Acknowledgements

This work was supported by NIH U01-AI-148119 to A.S.M. and F.N.

Author contributions statement

490 A.S.M. and F.N. conceived the study. A.L., P.V., and M.B. performed the experiments. A.S.M., S.L., and Z.C.T. performed the computational analysis. All authors reviewed the manuscript.

Figure Captions

495 **Figure 1: Profiling the binding effects of mixed-composition immune complexes.** a) Schematic of the immune complex (IC) binding experiment. Individual or mixtures of IgG subclasses are immobilized on multivalent TNP complexes. The binding of these complexes to CHO cells expressing a single Fc receptor is then quantified. b) Measured binding in relative fluorescence units (RFU) versus the previously reported affinity of each interaction. Only single subclass conditions are plotted. Error bars represent the
500 interquartile range of the measurements. c) The ratio of median binding quantified between valency 33 and 4, versus the reported affinity of the interaction. d) IgG1-IgG2 mixture binding to Fc γ RI shows appreciable binding, even though IgG2-Fc γ RI is documented to be non-binding. The RFU level here was normalized to match the Fc γ RI expression to the
505 Fc γ RIIIA-158F expression (shown in e) on CHO cells. e) IgG1-IgG4 mixture binding to Fc γ RIIIA-158F.

Figure 2: Principal component analysis (PCA) visualizes the variance in mixture binding measurements and their associated factors. a) Variance explained by each component in PCA. We found that the first two principal components (PC), PC1 and PC2,
510 can explain more than 93% of the variance in the measurement. b,c) Scores of PC1-PC2 for immune complexes of average valency 4 (b) and 33 (c); PC1 shows that most of the variance in data comes from 33-valent complexes, especially in IgG3. d) Loadings of PC1-PC2 indicate that PC2 is mostly associated with separating the allelic variants of Fc γ RIIA and IIIA. Fc γ RI and Fc γ RIIb points overlap.

515 **Figure 3: A multivalent binding model accurately accounts for *in vitro* binding of IgG mixtures.** a) Schematic of the multivalent binding model. b) Schematic of the process of predicting binding with documented affinities and inferring affinities from measurements. c) Measured versus predicted binding by the binding model with raw parameters. Points also vary in the IgG subclass used, which is not indicated. d) Binding model prediction with all
520 parameters but affinities fitted by Monte Carlo Markov Chain (MCMC). In (c) and (d), the IgG2-Fc γ RI outliers were circled in red. Since this interaction was previously reported as nonbinding, the actual predictions were all 0, only clipped to a nonzero value (1/10 of the next smallest value) to be plotted on logscale. e) Binding model prediction of all measurements (single and mixed IgG) with affinity inferred from single IgG measurements.

525 f) Binding model prediction of mixture IgG measurements with affinities updated with single
IgG measurements. g,h) Validate the updated affinities with a separate dataset¹⁶ by
predicting the binding with either documented (g) or updated (h) affinities. i-l) Predicted
binding of IgG4-IgG2 mixture to FcγRI (i,j) and IgG4-IgG3 mixture to FcγRIIB-232I (k,l),
with either documented (i,k) or updated affinities (j,l, solid line and left axis) compared with
530 measured binding (j,l, dashed line and right axis).

Figure 4: Inferred affinities from the binding data. a-d) The prior (documented)
distributions of binding affinities (assume all follow log-normal distributions) and posterior
(updated) affinities of IgG1 (a), IgG2 (b), IgG3 (c), and IgG4 (d). e) Updated affinities plot
against the binding measurements of single IgGs. Error bars represent the interquartile
535 range of the measurements. f) Updated affinities plot against the ratio of median binding
between valency 33 and 4 complexes.

Figure 5: Predict IgG effector cell binding with the multivalent binding model. a-d)
Measured *in vitro* binding of IgG1 (a), IgG2 (b), IgG3 (c), and IgG4 (d) IC of either 4- or 33-
valent to selective immune effector cells, classical (cMO) or nonclassical (ncMO)
540 monocytes and neutrophils (Neu). e-h) Model-predicted IgG1 (e), IgG2 (f), IgG3 (g), and
IgG4 (h) IC of 4- or 33- valent binding on each effector cell type under documented versus
updated affinities.

Figure 6: Perform *in vivo* target cell depletion regression on humanized mice. a)
Schematic of *in vivo* platelet depletion regression. To predict the percentage decrease of
545 platelet abundance after antibody injection in mice, we combined the binding model
predictions with Fc receptor and effector cell type weights, then transformed the sum into
depletion percentage with an exponential distribution cumulative density function. b-e)
Results of regression ran on documented (b,d) and updated (c,e) affinities: b,c) Actual vs.
predicted depletion of platelet; d,e) Predicted effector cell type weights; Error bars indicate
550 the interquartile range from MCMC runs.

References

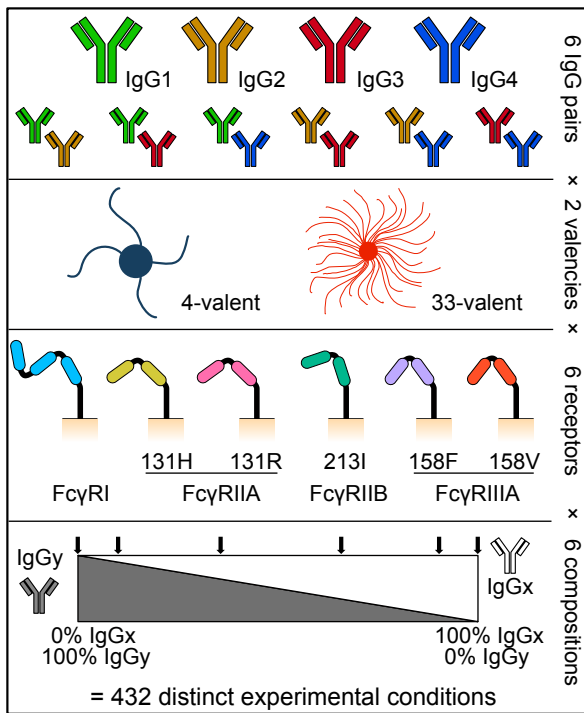
1. Nimmerjahn, F. & Ravetch, J. V. Divergent Immunoglobulin G Subclass Activity Through Selective Fc Receptor Binding. *Science* **310**, 1510–1512 (2005).
- 555 2. Dekkers, G. *et al.* Affinity of human IgG subclasses to mouse Fc gamma receptors. *mAbs* **9**, 767–773 (2017).
3. Bruhns, P. *et al.* Specificity and affinity of human Fcγ receptors and their polymorphic variants for human IgG subclasses. *Blood* **113**, 3716–3725 (2009).
4. Tan, Z. C., Orcutt-Jahns, B. T. & Meyer, A. S. A quantitative view of strategies to engineer cell-selective ligand binding. *Integr. Biol.* **13**, 269–282 (2021).
- 560 5. Deal, B. R. *et al.* Engineering DNA-Functionalized Nanostructures to Bind Nucleic Acid Targets Heteromultivalently with Enhanced Avidity. *J. Am. Chem. Soc.* **142**, 9653–9660 (2020).
6. Lux, A., Yu, X., Scanlan, C. N. & Nimmerjahn, F. Impact of Immune Complex Size and Glycosylation on IgG Binding to Human FcγRs. *J Immunol* **190**, 4315–4323 (2013).
- 565 7. Collins, A. & Jackson, K. A Temporal Model of Human IgE and IgG Antibody Function. *Front. Immunol.* **4**, (2013).
8. Higel, F., Seidl, A., Sörgel, F. & Friess, W. N-glycosylation heterogeneity and the influence on structure, function and pharmacokinetics of monoclonal antibodies and Fc fusion proteins. *Eur. J. Pharm. Biopharm.* **100**, 94–100 (2016).
- 570 9. Olivova, P., Chen, W., Chakraborty, A. B. & Gebler, J. C. Determination of N-glycosylation sites and site heterogeneity in a monoclonal antibody by electrospray quadrupole ion-mobility time-of-flight mass spectrometry. *Rapid Commun. Mass Spectrom.* **22**, 29–40 (2008).

- 575 10. Mimura, Y. *et al.* Glycosylation engineering of therapeutic IgG antibodies: challenges for the safety, functionality and efficacy. *Protein Cell* **9**, 47–62 (2018).
11. Biburger, M. *et al.* Monocyte Subsets Responsible for Immunoglobulin G-Dependent Effector Functions In Vivo. *Immunity* **35**, 932–944 (2011).
12. Montalvao, F. *et al.* The mechanism of anti-CD20–mediated B cell depletion
580 revealed by intravital imaging. *J. Clin. Invest.* **123**, 5098–5103 (2013).
13. Kerntke, C., Nimmerjahn, F. & Biburger, M. There Is (Scientific) Strength in Numbers: A Comprehensive Quantitation of Fc Gamma Receptor Numbers on Human and Murine Peripheral Blood Leukocytes. *Front. Immunol.* **11**, (2020).
14. Bakalar, M. H. *et al.* Size-Dependent Segregation Controls Macrophage
585 Phagocytosis of Antibody-Opsonized Targets. *Cell* **174**, 131-142.e13 (2018).
15. Tang, Y. *et al.* Regulation of Antibody-Dependent Cellular Cytotoxicity by IgG Intrinsic and Apparent Affinity for Target Antigen. *J. Immunol.* **179**, 2815–2823 (2007).
16. Robinett, R. A. *et al.* Dissecting FcγR Regulation through a Multivalent Binding Model. *Cell Syst.* **7**, 41-48.e5 (2018).
- 590 17. Lux, A. & Nimmerjahn, F. Of mice and men: the need for humanized mouse models to study human IgG activity in vivo. *J. Clin. Immunol.* **33 Suppl 1**, S4-8 (2013).
18. Crowley, A. R. & Ackerman, M. E. Mind the Gap: How Interspecies Variability in IgG and Its Receptors May Complicate Comparisons of Human and Non-human Primate Effector Function. *Front. Immunol.* **10**, (2019).
- 595 19. Bruhns, P. Properties of mouse and human IgG receptors and their contribution to disease models. *Blood* **119**, 5640–5649 (2012).
20. Tan, Z. C. & Meyer, A. S. A general model of multivalent binding with ligands of heterotypic subunits and multiple surface receptors. *Math. Biosci.* **342**, 108714 (2021).

21. Epstein, B. The Exponential Distribution and Its Role in Life Testing. (1958).
- 600 22. Schwab, I., Lux, A. & Nimmerjahn, F. Pathways Responsible for Human Autoantibody and Therapeutic Intravenous IgG Activity in Humanized Mice. *Cell Rep.* **13**, 610–620 (2015).
23. Siber, G. R., Schur, P. H., Aisenberg, A. C., Weitzman, S. A. & Schiffman, G. Correlation between Serum IgG-2 Concentrations and the Antibody Response to
605 Bacterial Polysaccharide Antigens. *N. Engl. J. Med.* **303**, 178–182 (1980).
24. Volkov, M. *et al.* Comprehensive overview of autoantibody isotype and subclass distribution. *J. Allergy Clin. Immunol.* **150**, 999–1010 (2022).
25. Nimmerjahn, F. & Ravetch, J. V. Translating basic mechanisms of IgG effector activity into next generation cancer therapies. *Cancer Immun.* **12**, 13 (2012).
- 610 26. Dekkers, G. *et al.* Decoding the Human Immunoglobulin G-Glycan Repertoire Reveals a Spectrum of Fc-Receptor- and Complement-Mediated-Effector Activities. *Front. Immunol.* **8**, 877 (2017).
27. Stone, J. D., Cochran, J. R. & Stern, L. J. T-Cell Activation by Soluble MHC Oligomers Can Be Described by a Two-Parameter Binding Model. *Biophys. J.* **81**, 2547–
615 2557 (2001).
28. Georgiev, I. S. *et al.* Delineating Antibody Recognition in Polyclonal Sera from Patterns of HIV-1 Isolate Neutralization. *Science* **340**, 751–756 (2013).
29. Lux, A. *et al.* A Humanized Mouse Identifies the Bone Marrow as a Niche with Low Therapeutic IgG Activity. *Cell Rep.* **7**, 236–248 (2014).
- 620 30. Chung, A. W. *et al.* Dissecting Polyclonal Vaccine-Induced Humoral Immunity against HIV Using Systems Serology. *Cell* **163**, 988–998 (2015).

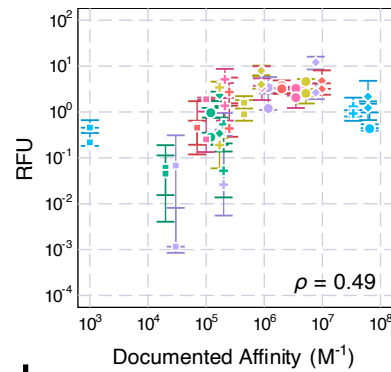
31. Lemke, M. M. *et al.* A systems approach to elucidate personalized mechanistic complexities of antibody-Fc receptor activation post-vaccination. *Cell Rep. Med.* **2**, 100386 (2021).
- 625 32. Ge, H., Xu, K. & Ghahramani, Z. Turing: A Language for Flexible Probabilistic Inference. in *Proceedings of the Twenty-First International Conference on Artificial Intelligence and Statistics* vol. 84 1682–1690.
33. Robinett, R. A. *et al.* Dissecting FcγR Regulation through a Multivalent Binding Model. *Cell Syst.* **7**, 41-48.e5 (2018).
- 630 34. Besançon, M. *et al.* Distributions.jl: Definition and Modeling of Probability Distributions in the JuliaStats Ecosystem. *J. Stat. Softw.* **98**, 1–30 (2021).
35. Whaley III, D. L. The interquartile range: Theory and estimation. (East Tennessee State University, 2005).
36. Mogensen, P. & Riseth, A. Optim: A mathematical optimization package for Julia. *J. Open Source Softw.* **3**, (2018).
- 635

a



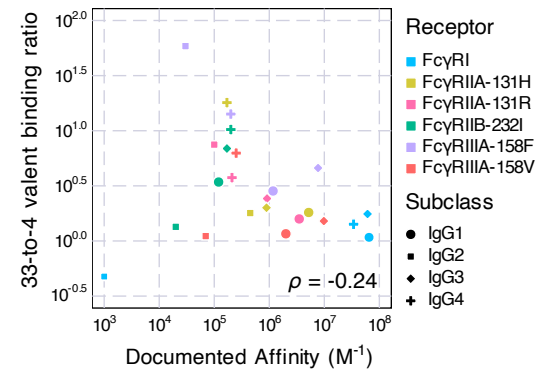
b

Documented affinity vs. single IgG binding



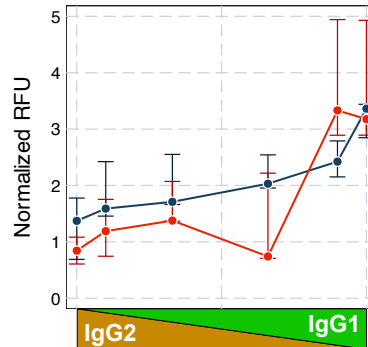
c

Documented affinity vs. intervalency ratio



d

IgG1-IgG2 mixture bind to FcγRI



e

IgG1-IgG4 mixture bind to FcγRIIA-158F

